Stability of spatial soliton arrays generated in a noninstantaneous Kerr medium from partially spatiotemporally coherent light

Gil Fanjoux, Eric Lantz, Fabrice Devaux, Hervé Maillotte

To be published in J. Opt. Soc. Am. B 2006

Stability of spatial soliton arrays generated in a noninstantaneous Kerr medium from partially spatiotemporally coherent light

Gil Fanjoux, Eric Lantz, Fabrice Devaux, and Hervé Maillotte

Institut FEMTO-ST, Département d'Optique PM Duffieux, Unité Mixte de Recherche, Centre National de la Recherche Scientifique, Université de Franche-Comté, n°6174 Route de Gray, 25030 Besançon Cedex, France

Received July 29, 2005; revised October 26, 2005; accepted November 3, 2005; posted January 9, 2006 (Doc. ID 63826)

We demonstrate numerically and experimentally how spatial soliton arrays generated through modulation instability in a planar waveguide with relaxing Kerr nonlinearity can be spatially and temporally destabilized when using a partially spatiotemporally coherent light pulse. However, the amplitude of the shot-to-shot spatial jitter is limited. This jitter depends on the correlation degree of the spatial noise between pulses, and this correlation degree strongly depends on the spatiotemporal coherence of the propagating beam.

OCIS codes: 190.3270, 190.4420, 190.5530, 190.3100, 030.1640.

1. INTRODUCTION

Spatial modulation instability (SMI) is induced by the interplay between nonlinearity and linear diffraction during propagation of an intense and spatially extended beam in a nonlinear medium.[1] More precisely, it corresponds to parametric amplification of preferred spatial frequencies initially present in the weak spatial noise of the propagating beam. Under specific conditions, SMI (or its equivalent in the time domain) can lead to the formation of arrays of bright peaks in the transverse dimension that have characteristics similar to those of solitons.[2–8] As Kerr solitons can be stable only in a (1+1)-dimensional geometry,[9–11] studies on spatial Kerr soliton arrays are generally made in a planar waveguide.[12–14] For an ideal instantaneous Kerr medium, the period of the array is given by the spatial frequency corresponding to the highest modulation instability (MI) gain, which depends on the beam intensity launched into the waveguide.[12] Therefore, this input intensity is naturally the main parameter that must be controlled to generate soliton arrays. However, other subtle parameters can strongly influence the spatiotemporal dynamics of spatial soliton arrays such as the nonlocality of the nonlinearity,[13] the relaxation time of the Kerr nonlinearity,[14–17] and the coherence of the input beam.[11,18–23]

Previous works have shown the decisive and interlinked role of relaxation time of the medium and of the coherence of the input beam in the emergence of SMI. By injecting purely coherent light in a nonlinear medium, SMI can be totally annihilated by dynamic noise present in the injected beam if the medium is noninstantaneous,[16,17] whereas SMI is absolutely not affected if the medium is instantaneous. On the other hand, theoretical[19,20] and experimental works[11,21–23] have proved that SMI can occur with spatially and temporally incoherent light only in noninstantaneous nonlinear media (photorefractive crystals in all of these references). Incoherent SMI indeed occurs, like for incoherent soliton generation, when the response time of the nonlinear medium is larger than the average time of the phase fluctuations across the beam. To resume, the noninstantaneity of the medium plus a dynamic noise (purely coherent) can stop SMI despite a positive growth rate,[17] whereas SMI seeded by incoherent light in noninstantaneous media can be arrested by the negative growth rate when the nonlinearity is smaller than a certain coherence-dependent threshold.[19] Partially incoherent temporal MI has also been recently demonstrated in an instantaneous Kerr medium (optical fibers).[24,25] Then the relaxation time of the medium and the coherence of injected light are essential parameters for the existence of the MI.

In direct relation with this work, i.e., SMI in a Kerr medium with pulsed illumination, previous studies of soliton array generation from a spatially extended laser beam, coherent spatially (but noisy or weakly modulated) and temporally,[14,15] have demonstrated that a finite relaxation time allows the spatial period of the soliton array to be maintained along the pulse. This is in contradiction with standard MI theory in an instantaneous Kerr medium because the instantaneous intensity varies (pulsed light), which should lead to a variable spatial period. This peculiar temporal feature is of primary importance to understand the dynamics and stability of soliton array formation and propagation.[15] This dynamics indicates that SMI in a relaxing Kerr medium amplifies preferentially spatial frequencies present at the front of the soliton array, and these spatial frequencies determine and maintain the array spatial period all along the coherent pulse. As regards influence of the spatiotemporal coherence of the input beam, we numerically showed[18] that SMI occurs if the spatially noisy beam launched into the waveguide presents a minimum degree of spatial coherence. Moreover, if SMI starts from a weak spatial noise totally uncorrelated from one shot to another, a completely random

transverse jitter of the soliton arrays should be observed at the waveguide output. Now, if the input pulse also holds temporal noise, it is necessary to correlate the temporal slices of this pulse to maintain the soliton arrays all along the single pulse. Otherwise the time-integrated output beam would exhibit completely blurred soliton arrays. To avoid this, if the soliton arrays are generated in an instantaneous medium, the beam at the waveguide input has to be temporally coherent. On the other hand, if the relaxation time of the Kerr medium is of same order of magnitude as the pulse duration, the correlation of the temporal slices is provided by the relaxation itself.

Note that the bond between random noise and random pattern position has been already observed in a quadratic medium. Experimental studies have indeed shown that spatially or spatiotemporally noisy input beams can generate a solitonlike pattern in quadratic crystals,[8,26] with spatial positions that evolve randomly from shot to shot and with input intensities equal to many times the single soliton threshold.[27]

The aim of the present work is to understand the role of the spatiotemporal characteristics of the noise on the SMI dynamics, either in each injected pulse (i.e., spatiotemporal coherence) or for consecutive pulses (i.e., degree of correlation). Two previous experimental studies have already gained partial knowledge on the role of coherence on the stability of soliton arrays in a nonlinear Kerr planar waveguide. For spatiotemporally coherent input beams, deterministic spatial frequencies predominate, due to defects of the waveguide or deterministic noise in the pump laser beam. Then, as observed in a relaxing medium (CS_2),[15] SMI starts from these frequencies and, in addition to being maintained along one pulse, the soliton arrays are therefore spatially stationary from one shot to another. Conversely, in an instantaneous Kerr material (AlGaAs), the authors of Ref. 12 observed intensity-dependent shallow MI spikes that jitter from one shot to another when injecting pulses delivered by an optical parametric generator. These less-coherent pulses present some amount of amplified spatiotemporal quantum noise, and therefore the amplitude of the spatial jitter could not be controlled as it comes from the intrinsic random spatial noise of the injected beam. Note that, as mentioned above, the observation of arrays of spikes imposes that the input beam should have a minimal degree of spatial coherence and a rather high degree of temporal coherence as the medium is considered instantaneous.[18]

The present work bridges a gap between these two previous studies.[12,15] Starting from the coherent and stable situation of Ref. 15, we study how a partially spatiotemporally incoherent beam can destabilize the soliton arrays generated in a noninstantaneous Kerr medium and causes their shot-to-shot jittering. For that purpose, according to Refs. 12 and 18, the injected field has to present partial spatial incoherence to initiate SMI from truly random spatial noise frequencies. Purposely, we use in this work spontaneous parametric downconversion (SPDC) as a spatiotemporally incoherent noise source. As SPDC corresponds to amplified quantum noise, this spatially incoherent noise is intrinsically random shot to shot. Thanks to SPDC, we have experimentally observed a shot-to-shot random spatial jitter of the soliton arrays. However, the jitter amplitude is limited even if the random noise is larger than the deterministic noise due to the experimental setup. We discuss in this paper the influence of a weak purely spatial deterministic noise on the jitter amplitude. Furthermore, as SPDC is also temporally incoherent, this work allows one to study the interaction between the temporal incoherence of the propagating pulse and the relaxation time of the medium. We demonstrate here the formation of twisting soliton arrays due to the action of both parameters.

The paper is divided in four sections. Section 2 is devoted to the experimental setup performed with two different configurations. Section 3 presents the parameters of the numerically simulated experiment. Then numerical and experimental results are presented and discussed in Section 4, with special emphasis on the observed limitation of the spatial jitter of the soliton arrays.

2. EXPERIMENTAL SETUP

The experimental setup is shown in Fig. 1. SPDC is generated in a type 1 β-barium borate (BBO) crystal cut for collinear phase matching at degeneracy with $L_{cx} \times L_{cy} \times L_{cz} = 5\ \text{mm} \times 5\ \text{mm} \times 10\ \text{mm}$. The 3 cm long Kerr planar waveguide is formed by a thin space between two SK5 linear glass blocks (linear refractive index of 1.59 at $\lambda = 532$ nm) filled by a CS_2 nonlinear liquid (linear refractive index $n_0 = 1.64$; nonlinear Kerr index $n_2 = +3.5 \times 10^{-18}\ \text{m}^2/\text{W}$). The thickness $d \cong 10\ \mu\text{m}$ of the waveguide, that corresponds therefore to a multimode structure, has been chosen to obtain isotropic waveguiding (i.e., negligible linear birefringence) and, more importantly, to decrease spatial deterministic noise brought about by the waveguide defects.

The 532 nm (266 nm) beam is delivered by a frequency-doubled (frequency-quadrupled), Q-switched, and mode-locked Nd:YAG laser with a 10 Hz repetition rate and a pulse duration (FWHM) equal to 38 ps (27.5 ps). To ensure efficient coupling within the waveguide, the elliptic profiles of the beams are shaped by cylindrical lenses so that the beam waists approximately equal the thickness d. Then the whole beam is selectively launched into the fundamental mode by using an afocal optical system ($\times 1$ magnification) that images the output of the BBO crystal onto the waveguide input plane. This afocal system has a numerical aperture inferior to the single-mode aperture ($\text{N.A.} \leqslant \lambda/2d$) while it preserves the inclination of the wave vectors of SPDC between the BBO output and the waveguide input. All beams entering the waveguide are horizontally polarized so as to excite the TE_0 mode. This requires a lower input energy to achieve the soliton regime compared with the TM_0 mode[28] and provides polarization stability during propagation by avoiding energy exchange between the TE and TM modes.[29]

At the waveguide output, two synchronized single-shot CCD cameras acquire the time-integrated output face image and its Fourier spatial spectrum for the same single laser shot.

Note that special care has been taken to avoid seeding of stimulated Raman scattering by the SPDC beam launched into the waveguide. Indeed, despite a 1 cm long BBO crystal (which should lead to a 18 nm narrowband

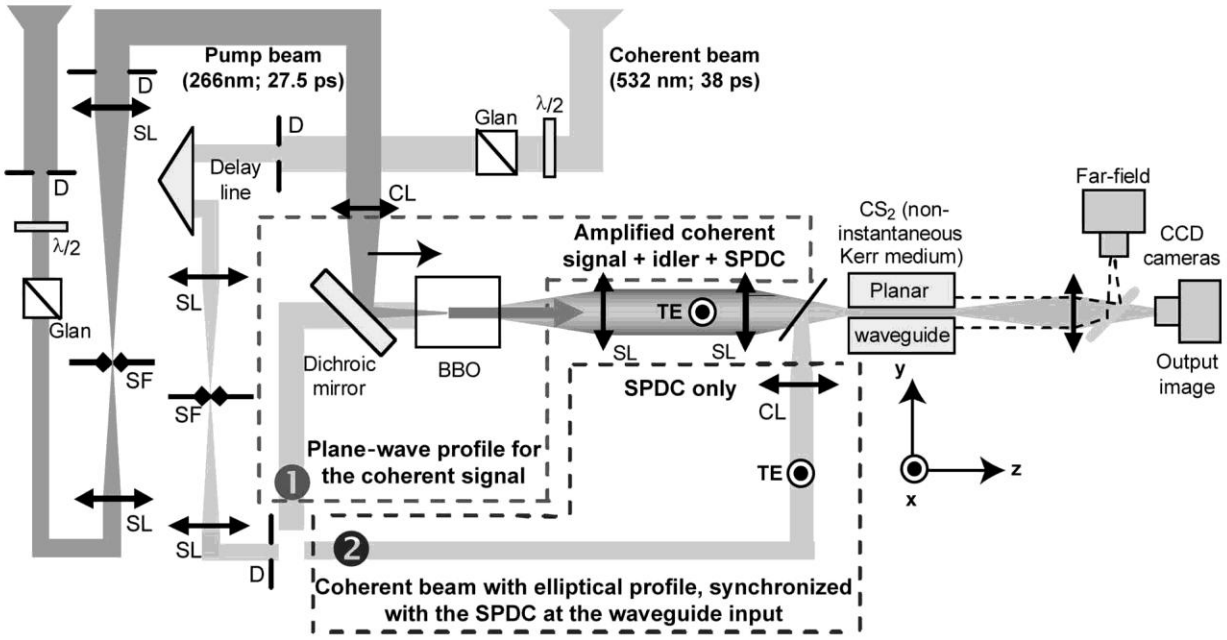

Fig. 1. Experimental setup. CL, cylindrical lenses; SL, spherical lenses; D, diaphragm; SF, spatial filter. Both experimental configurations 1 and 2 are represented.

SPDC temporal spectrum), the short effective length due to strong focusing of the 266 nm pump beam leads to wideband SPDC (more than 100 nm for the highest spatial frequencies), as experimentally observed. So, when launching a SPDC intensity that is too high, we have clearly observed the first Raman Stokes order (at 551 nm in CS_2) at the waveguide output. As Raman emission yields random spatial intensity fluctuations that could be superimposed on the soliton array generated at 532 nm, this could lead to misleading interpretations of our results. We have thus carefully checked that Raman emission was absent in all our measurements.

As SPDC is totally incoherent, it cannot generate soliton arrays alone[18] and must be then superimposed on a coherent pump beam. For that purpose, two different experimental configurations have been used. In the first one, already used in the numerical simulations of Ref. 18, the weak plane-wave coherent signal (532 nm) and pump (266 nm) beams, spatially superimposed and temporally synchronized, are collinearly injected in the BBO crystal under the phase-matching angle (configuration 1 in Fig. 1). The field at the BBO output, formed by the amplified coherent signal plus the idler plus the SPDC, is then directly injected into the CS_2 waveguide through the afocal imaging system. The great advantage of this experimental configuration is intrinsic spatiotemporal superimposing of the coherent (amplified signal plus idler) and incoherent (SPDC) beams at the BBO output. They indeed have the same duration ($\sim$10–12 ps) and the same transverse elliptical sizes since the spatiotemporal profile is given by the 266 nm pump beam. Unfortunately, parametric amplification of the coherent signal is sensitive to the relative phase variation between the pump and the input signal. So, the BBO output beam at 532 nm actually presents rough variations of, first, its intensity level and, second, the coherent/SPDC ratio, which precludes from controlling both of these features experimentally with the 10 Hz pulsed laser. These features are yet crucial for soliton array generation because the input intensity determines the array period in a certain extent, and tuning of the coherent/incoherent ratio determines the spatial degree of coherence of the input beam. Nevertheless, despite a low reproducibility of the results due to a large number of inappropriate shots, a statistical analysis on the favorable events leads us to observe a limited spatial jittering of the soliton arrays (see Subsection 4.A), in accordance with our numerical simulations.

To control the intensity and the coherent/incoherent ratio at the waveguide input, the second experimental configuration (labeled 2 on Fig. 1) separates the coherent and incoherent optical paths before mixing both beams at the waveguide input. Therefore, only SPDC is generated in the BBO crystal. It is important to note that SPDC is now shorter than the coherent 532 nm beam (38 ps), first because the 266 nm pump has a duration equal to 27.5 ps and second because parametric generation further shortens SPDC to $\sim$10–12 ps. The SPDC pulse is then temporally synchronized by an optical delay line and spatially superimposed on the coherent beam at the waveguide input with a pellicle beam splitter whose 2 μm thickness avoids double reflection ($T \cong 90\%$ for SPDC and $R \cong 10\%$ for the coherent beam). Special care has been taken to inject both beams on the same waveguide mode, with perfectly collinear directions so as to avoid interference fringes between the coherent beam and a possible residual 532 nm radiation within the 266 nm pump. Indeed, even with a very low contrast, some interference patterns can induce SMI,[14] and the spatial jitter in this case would correspond to the random-phase variation between the coherent and the residual 532 nm beams. Note that the coherent beam is rather stable shot to shot ($\sim$5% energy fluctuations). On the other hand, SPDC presents strong variations because of the intrinsic random nature of the amplified quantum noise. However, as the SPDC level has

to be much less powerful than the coherent beam in our study, the energy variation at the waveguide input remains limited.

3. NUMERICAL SIMULATIONS

We summarize here the numerical simulations that have been already described in Refs. 14 and 18.

SPDC corresponds to amplification by a strong pump pulse of quantum fluctuations of the vacuum field (i.e., the quantum noise), even when no input signal is injected in the crystal. Numerically, a white noise with a random phase and Gaussian-distributed amplitude, corresponding to a mean energy of half a photon per spatiotemporal mode, simulates this quantum noise. Propagation and amplification in the quadratic BBO crystal are simulated from the classical coupled-wave equations of the three-wave-mixing interaction.[18,30] Numerically, for each step Δz, propagation and amplification of the input field are performed in two steps. The quantum noise field is first amplified in the direct space. Second, the input fields (quantum noise plus pump) are propagated in Fourier space by taking into account the phase-mismatch contributions of diffraction and of linear dispersion due to the group-velocity difference between the pump and the signal (temporal walk-off). In other words, the phase mismatches are calculated for all spatial and temporal frequencies contained in the corresponding numerical frequency bands. Pump depletion is also taken into account.

Scalar propagation in the single-mode planar Kerr waveguide is modeled by the usual (1+1)-dimensional nonlinear Schrödinger equation (NLSE) that governs the spatiotemporal propagation of solitons in a steady-state regime[31] assuming a lossless and dispersionless nonlinear medium, and neglecting modal birefringence. To take into account the 2 ps decay time of the Kerr nonlinearity in CS_2 due to relaxation of molecular reorientation, the NLSE is modified by convoluting the nonlinear index response with a decreasing Debye-type exponential function defined for positive time (assuming instantaneous rise time and finite relaxation).[14,15] The numerical simulation uses the standard split-step Fourier-transform algorithm already used and described in Refs. 14 and 15.

For this study, we numerically inject in the waveguide a wide coherent beam with a noiseless, temporally coherent Gaussian pulse envelope, and with a weak purely spatial noise, identical shot to shot, superimposed on a SPDC beam of similar sizes, which is spatiotemporally incoherent and random shot to shot.

4. NUMERICAL AND EXPERIMENTAL RESULTS

The whole beam propagating into the 3 cm long waveguide (coherent plus SPDC) always presents some deterministic spatial intensity and phase noise, constant along a single pulse and also from one shot to another. If this noise predominates as in the purely coherent case, SMI amplifies the corresponding deterministic spatial frequencies. As a result, the generated soliton array exhibits a tiny or even null spatial jitter[15] (see Fig. 13 below). However, even when the contribution of random noise in the MI-amplified spatial-frequency bandwidth is much larger than that of deterministic noise, our study shows that other physical processes limit the amplitude of the shot-to-shot random jitter of the SPDC-driven spatial soliton array.

A. Experimental Configuration 1

A strong limitation in the jitter amplitude is due to the fact that, for comparable noise levels, time integration of the purely deterministic spatial noise (that is therefore purely temporally coherent) over the relaxation time of the Kerr medium gives a greater contribution to soliton array formation than time integration of the spatiotemporal SPDC noise, which is temporally uncorrelated. We have numerically verified this behavior by considering identical SPDC and coherent pulse durations, 10 ps for both, which corresponds to experimental configuration 1. The amplitude of the deterministic spatial noise is 0.7% of the coherent pulse maximum amplitude while the amplitude ratio SPDC/coherent peak is $\sim 29 \times 10^{-3}$. Figure 2 shows the spatial-frequency spectra, time integrated over a 2 ps relaxation time, of the coherent and SPDC pulses at the waveguide input, whereas Fig. 3 shows the same spectra for a single temporal slice at the peak of the pulse. To help the comparison, the intensity scales in Figs. 2 and 3 have been chosen so as to keep the same relative level for the coherent noise (black curves). From these figures, it is clear that the coherent/incoherent noise ratio increases when time integrating. In Fig. 3, SPDC energy is shared between some highly intense spatial frequencies. At the opposite, in Fig. 2, its energy is spread all over the spatial-frequency range. Figure 4(a) shows the waveguide output intensity profiles for five different shots having the

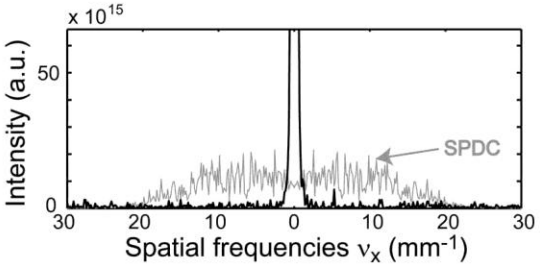

Fig. 2. Time-integrated spatial-frequency spectra of both deterministic and random contributions at the waveguide input, coherent beam (black curve) and SPDC (gray curve) with a pulse duration equal to 10 ps for both the SPDC and the coherent beams.

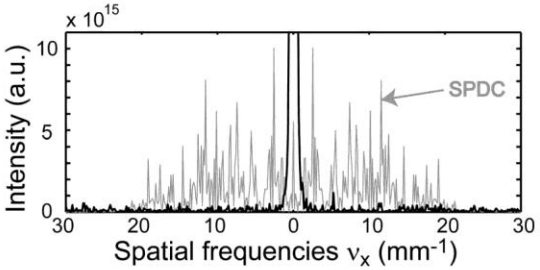

Fig. 3. Single temporal slice of spatial-frequency spectra of both contributions at the peak of the 10 ps pulse entering the waveguide, coherent beam (black curve) and SPDC (gray curve).

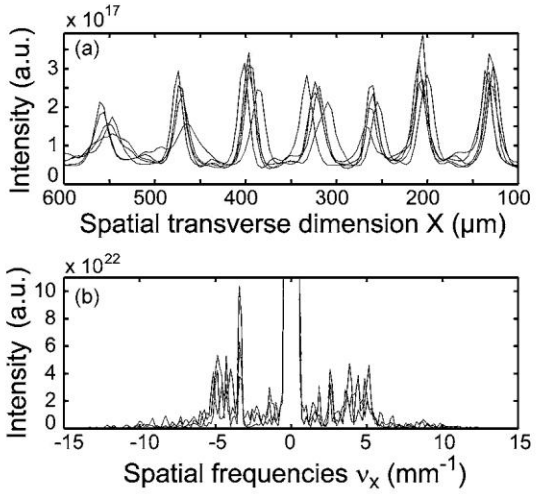

Fig. 4. Numerical results for five laser shots with the same 10 ps pulse duration for the coherent and SPDC beam and with the input spatial-frequency spectra of Figs. 2 and 3: (a) time-integrated waveguide output intensity profiles, (b) corresponding time-integrated spatial spectra.

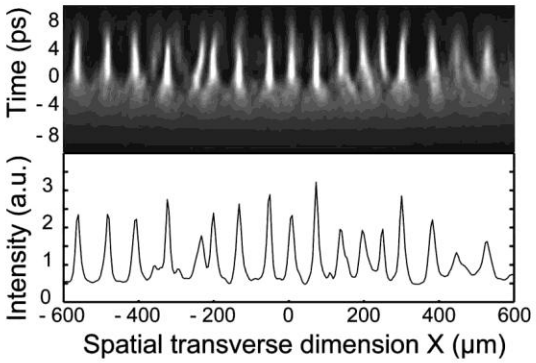

Fig. 5. Corresponding spatiotemporal pattern and time-integrated profile for a single shot at the waveguide output.

same noise characteristics as those of Figs. 2 and 3. Although the corresponding spectra of Fig. 4(b) effectively show some randomness in the amplified spatial frequencies, the spatial jitter of such SPDC-driven soliton arrays is not totally random, however. Time integration of the spatial noise, due to the relaxation time that correlates the temporal slices, i.e., increases the temporal coherence of the propagating pulse, is responsible for this jitter limitation.

Now, the SPDC level can be raised to increase spatial incoherence, which should lead us to observe a larger jitter. However, temporal incoherence also increases at the same time, which affects the maintaining of the soliton array even along a single pulse. A lower temporal coherence leads to temporal twisting of the solitons, or even their splitting. Indeed, correlation of the temporal slices by the relaxation time is efficient on 2 ps typically. Therefore, contrary to Ref. 15 where the injected laser beam was temporally coherent, the relaxation time here does not maintain the solitons all along the pulse, but only on temporal coherence cells of 2 ps duration. Figures 5 and 6 show the spatiotemporal and time-integrated patterns at the waveguide output for two different degrees of temporal coherence. The SPDC/coherent amplitude ratio is 29 $\times 10^{-3}$ in Fig. 5 and 50×10^{-3} in Fig. 6. It is clear that temporal incoherence destroys the maintaining of the soliton array along the pulse. Hence, time integration of the pulse at the waveguide output presents a blurred profile as the temporal twisting widens the time-integrated soliton profiles, and additional spatially shifted peaks even appear when temporal splitting of the soliton array occurs. In conclusion, an important shot-to-shot jitter of the time-integrated soliton array is not observable in a relaxing medium due to the time integration effect on the relaxation time for low SPDC levels and due to the twisting effect on one pulse for a high SPDC level.

In an instantaneous Kerr medium, such spatial blurring and then the shot-to-shot transverse jitter should be much more important, as the successive temporal slices of one pulse are totally independent and can be considered as uncorrelated events. They then form uncorrelated arrays of spikes at different transverse spatial positions when temporal coherence is low.[18] To verify this, numerical simulations have been made with exactly the same parameters as above but with the relaxation time put to zero. Figure 7 presents output profiles corresponding to five successive temporal slices positioned near the peak of one pulse. At the waveguide input, each slice presents a spatial-frequency spectrum comparable to that of Fig. 3. It is clear that the spatial positioning at the waveguide output is now random, despite the presence of some deterministic noise. Then the time-integrated waveguide output is totally blurred. However, as the correlation between each spatial position of the successive soliton arrays is given by the temporal coherence of the pulse, the blurring level strongly depends on this parameter. Thus, if the temporal coherence increases, the blur would decrease and some peaks would appear above a broad background, as observed in Ref. 12.

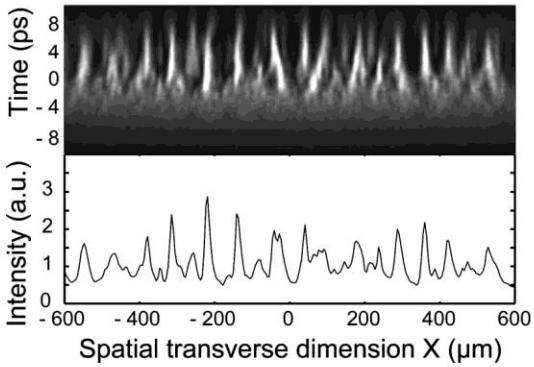

Fig. 6. Spatiotemporal and single-shot time-integrated patterns at the waveguide output with a smaller degree of temporal coherence than for Fig. 5.

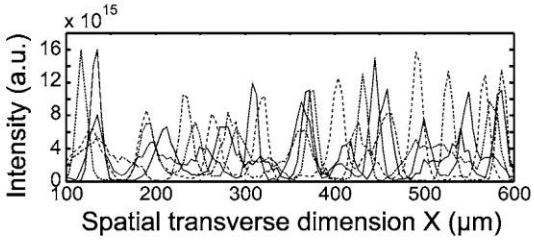

Fig. 7. Profiles generated by five successive temporal slices of one pulse after propagation in an instantaneous medium.

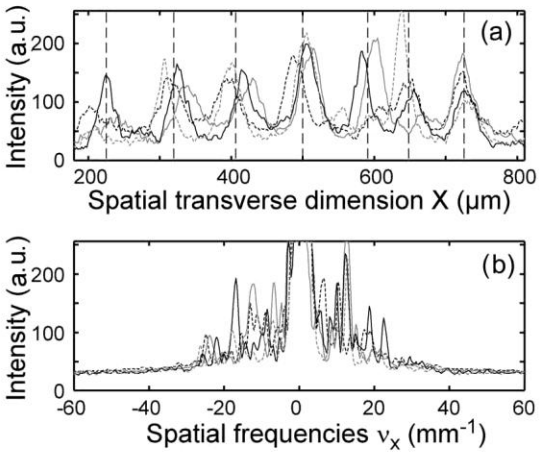

Fig. 8. Experimental measurements of the shot-to-shot jitter of the soliton array in experimental configuration 1.

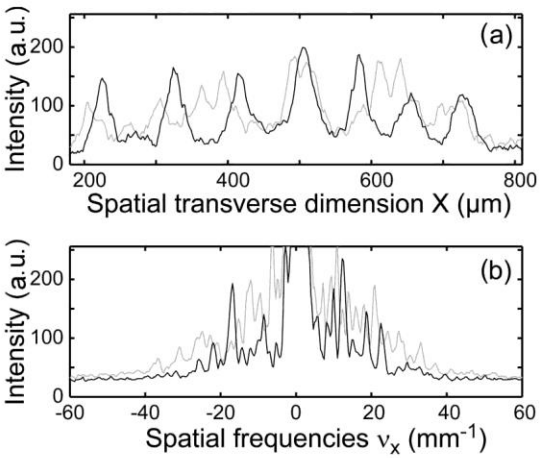

Fig. 9. Another experimental observation with the same experimental conditions as for Fig. 8.

Experimental measurements are presented in Figs. 8 and 9. Even if we are lacking control on the coherent/SPDC ratio and beam energy at the waveguide input, we have selected waveguide outputs that present approximately the same energy and the greatest spatial jitter. It is important to note that these experimental data come from one series being composed of approximately 20 measurements. Hence, they are obtained without any change in the experimental setup. Figure 8 shows four shots that point out the maximal observable jitter of the soliton array. As in the simulations where time integration of the spatial noise limits the transverse jitter, this experimental jitter is not totally random and the peaks oscillate around a mean position marked by the dashed curves in Fig. 8(a). The spatial-frequency spectra in Fig. 8(b) show multiple peaks and are different from one shot to another, which confirms the shot-to-shot random nature of the SPDC-driven MI process. Now, for some laser shots in the same series, the coherent/SPDC ratio seems to be smaller. Figure 9(a) shows one soliton array of Fig. 8 compared with an output profile exhibiting some peaks without any periodicity. In the spatial-frequency domain [Fig. 9(b)], the corresponding black spectrum of the soliton array exhibits some clear peaks around 12 mm^{-1} (=1/84 μm^{-1}), whereas the energy is spread in several spatial frequencies for the gray blurred array. This irregular profile in Fig. 9(a) presents similarities with the time-integrated waveguide output shown in Fig. 6, such as a widened soliton peak [near $x=500$ μm in Fig. 9(a) and $x=-10$ μm in Fig. 6] and additional peaks [near $x=400$ μm in Fig. 9(a) and $x=+50$ μm in Fig. 6] that could be induced by temporal twisting or splitting of the soliton array, respectively, when temporal incoherence increases.

B. Experimental Configuration 2

We have implemented experimental configuration 2 to better control the spatial destabilization of the soliton array by the spatiotemporally incoherent SPDC beam. Moreover, the different durations of the SPDC and coherent pulses in this case give an additional degree of freedom to study more precisely the dynamical contribution of spatiotemporal partial incoherence on the stability of the soliton array. Indeed, the fact that the incoherent part (SPDC) is shorter than the coherent part in the launched pulse implies that the MI-amplified spatial frequencies come from different noise sources. The noise that will govern the dynamics depends on the relative temporal position of the SPDC short pulse with respect to the front part of the soliton array generated by the longer coherent pulse. The SPDC pulse is experimentally tuned by the delay line while the temporal position of the front of the soliton array depends on the input intensity for a fixed propagation length.[15] Different cases are then possible. First, if SPDC is temporally synchronized with the trailing edge of the coherent pulse, SMI cannot start from random spatial frequencies, and therefore the soliton array never presents shot-to-shot spatial jitter. Second, if SPDC is positioned at the peak of the coherent pulse, SMI preferentially amplifies spatial frequencies in this part of the pulse at the beginning of the propagation, which would involve spatial jitter of the soliton array. However, if the propagation length is sufficient, the front of the soliton array moves toward the leading edge of the pulse[15] where the ratio SPDC/deterministic noise is lower. As the relaxation time of the medium imposes the spatial period in the following temporal slices, the transverse position of the soliton array becomes therefore more stable. The last case corresponds to SPDC positioned on the leading edge of the coherent pulse. At the beginning of the propagation, SMI starts from spatial frequencies at the peak of the coherent pulse, i.e., predominantly deterministic. However, for a sufficient input intensity, the front of the soliton array moves forward and reaches the temporal part of the pulse where SPDC is maximal. SMI then amplifies random spatial frequencies and the spatial jitter should therefore be observable.

In the numerical simulations, the input corresponds to a coherent beam (38 ps) with a purely deterministic, constant shot-to-shot spatial noise whose amplitude corresponds to 0.7% of the pulse maximum amplitude, superimposed on the SPDC beam (10 ps) bearing random spatiotemporal noise with a ratio SPDC/coherent peak equal to $\sim 29\times10^{-3}$. The only varying parameter is the delay between the SPDC and the coherent pulses as shown in Fig. 10. Note that both profiles are normalized to 1 in this figure. Four different delays equal to +11 ps

(SPDC is late compared with the coherent pulse), 0 ps (coincident maxima), −11 ps, and −22 ps have been used. The intensity of the coherent beam is sufficiently high to allow moving the front of the soliton arrays toward the leading edge of the pulse on the 3 cm propagation length. Figure 11(a) shows that, in the absence of SPDC, the time-integrated profiles of five different laser shots at the waveguide output are perfectly superimposed while Fig. 12(a) represents the corresponding spatiotemporal pattern for one of these shots, which we will call the coherent soliton array in the following. Note that the zero graduation of the temporal axis in Fig. 12(a) corresponds to the peak of the coherent pulse at the waveguide input. However, because of the relaxation time of the Kerr medium, this peak is slightly shifted toward the trailing edge of the pulse, which leads to the sliding of all the temporal envelopes to the rear, as is clearly visible in Figs. 12(a)–12(e). The time-integrated output profiles for five shots with the different delays between the coherent and the SPDC pulses are shown in Figs. 11(b)–11(e). It is clear that the

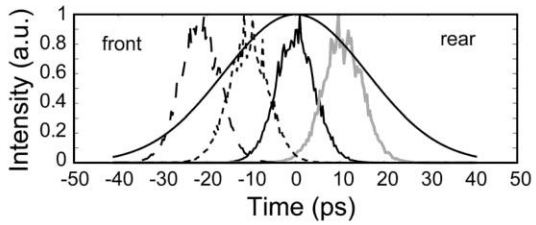

Fig. 10. Temporal adjustment between the coherent (38 ps) and the SPDC (10 ps) pulses with delays equal to +11 ps (gray curve), 0 ps (solid curve), −11 ps (dotted curve), and −22 ps (dashed curve). All profiles are normalized to 1.

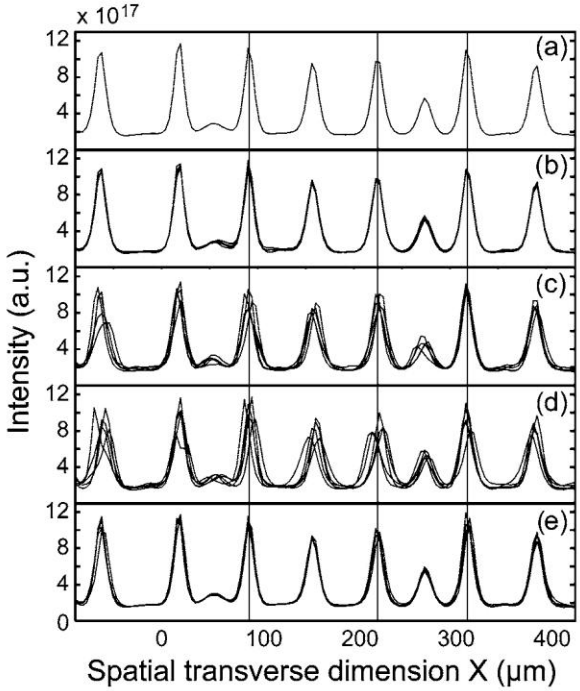

Fig. 11. Time-integrated waveguide output profiles corresponding to an input beam composed of (a) the coherent pulse without SPDC and the coherent pulse superimposed with SPDC with delays equal to (b) +11 ps, (c) 0 ps, (d) −11 ps, (e) −22 ps. Five shots are superimposed on each image.

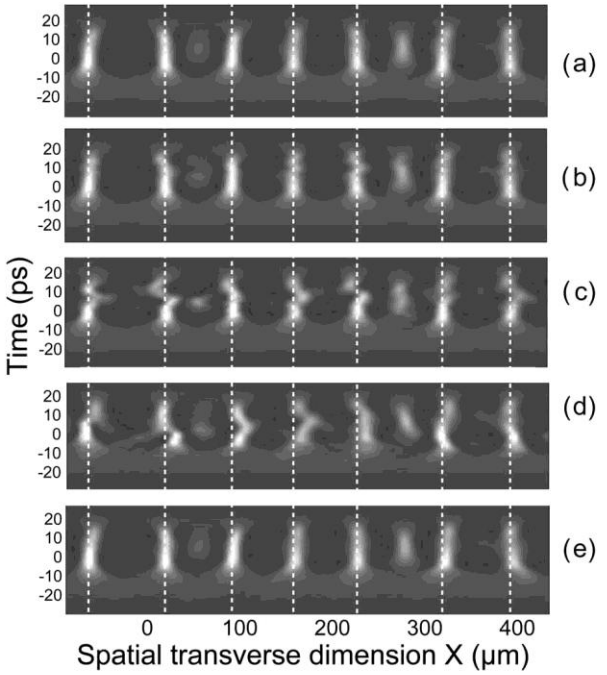

Fig. 12. Spatiotemporal output pattern for one of the shots of Fig. 11. The vertical white dotted lines indicate the position of the peaks of the coherent spatial soliton array.

spatial jitter of the soliton arrays depends on this delay. Note that Fig. 11(d), for which the delay equals −11 ps, shows the largest jitter, in agreement with the above discussion, because the front of the soliton arrays has moved forward where SPDC is the highest. For a further advance, however, [Fig. 11(e)], the total instantaneous intensity (coherent part plus SPDC) is no more sufficient at the beginning of the pulse and the soliton array forms behind in a much more stable way, where the coherent part dominates the dynamics.

Moreover, as spatiotemporal coherence decreases in the temporal slot where the SPDC and coherent pulse are superimposed, the coherent part of the soliton array is not correlated by the relaxation time to the part perturbed by the shorter SPDC pulse. This consequently leads to a transverse spatial shift of the solitons during the pulse. This behavior is clearly visible in the single-shot spatiotemporal patterns of Figs. 12(b)–12(d). For example, in Fig. 12(c) where SPDC is synchronized with the top of the coherent pulse, the front of the array corresponds approximately to the coherent soliton array, whereas its end is perturbed by SPDC, and then presents twisting solitons. At the opposite, in Fig. 12(d) where SPDC is synchronized with the front of the coherent pulse, it is the rear part of the soliton array that seems to correspond to the coherent soliton array, whereas the front part shows the spatial jitter seeded by SPDC.

In conclusion, the most favorable case in which to observe maximal spatial jitter corresponds to SPDC temporally positioned approximately in the front of the soliton arrays. In other words, this is when the spatial coherence is the lowest in the temporal part of the pulse where SMI is the most efficient. However, as the longer coherent temporal part of the soliton array conserves the spatial position from one laser shot to another, because of the deter-

ministic noise contribution, the spatial jitter must be lower than in experimental configuration 1 for the same coherent/SPDC ratio.

Experimental measurements are shown in Figs. 13 and 14. Figure 13 shows three consecutive laser shots with only the coherent beam injected in the waveguide (without SPDC). It is clear in Fig. 13(a) that the soliton arrays are perfectly superimposed, in agreement with previous work.[15] This implies that SMI starts from deterministic noise with amplification of identical spatial frequencies with the same intensity and the same phase, as confirmed by the perfect superimposition of the three spatial spectra in Fig. 13(b). This is also confirmed by the observation of the waveguide output in a linear regime (low input intensity) where spatial noise is totally deterministic shot to shot: By comparing the input beam with the output beam, we have observed that the deterministic noise is essentially due to the waveguide and is therefore extremely difficult to reduce. As a confirmation, a small translation of the waveguide in spatial transverse direction X leads to an equivalent translation of the soliton arrays, which

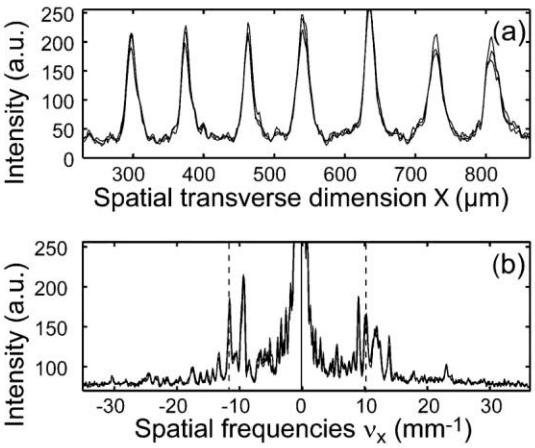

Fig. 13. Experimental time-integrated waveguide output profiles of soliton arrays without SPDC for three consecutive laser shots: (a) output image, (b) the corresponding experimental spatial-frequency spectra.

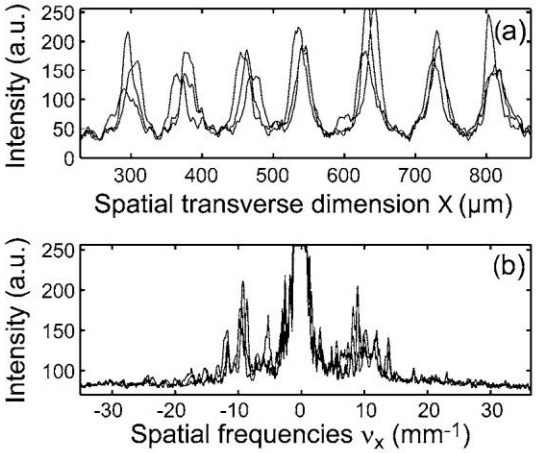

Fig. 14. Experimental time-integrated waveguide output beams of soliton arrays with SPDC superimposed on the coherent beam at the waveguide input for three consecutive laser shots: (a) output image, (b) the corresponding experimental spatial spectra.

clearly implies that SMI amplifies spatial frequencies coming preferentially from the waveguide defects even though the SK5 glass blocks that constitute the waveguide are polished at $\lambda/20$.

Now, when SPDC is added to the coherent beam, both the deterministic noise and the superimposed shot-to-shot random spatial noise are clearly observable at the waveguide output in a linear regime. In a nonlinear regime, a spatial jitter of the soliton arrays in the transverse dimension is observed, as shown in Fig. 14(a). The three different spatial spectra in Fig. 14(b) confirm that SMI has started from different spatial frequencies. Note that the images without and with SPDC (Figs. 13 and 14, respectively) have been successively recorded (with a shutter closed or open on the SPDC beam path), i.e., with exactly the same experimental setup, the same 266 nm pump and coherent 532 nm beam energy. To optimize the spatial jitter of the soliton arrays, we have tuned precisely the delay line on the coherent beam path for a fixed input energy injected in the waveguide. Figure 14(a) actually presents the maximal spatial jitter observed in our experiments. This jitter is always lower than in experimental configuration 1, which confirms the results of the numerical simulations. Indeed, both the previously discussed time integration effect plus the influence of the coherent/SPDC synchronization occur, which strongly limits the spatial jitter of the soliton arrays in configuration 2.

5. CONCLUSION

This work presents a comprehensive numerical and experimental study of the role of partial spatiotemporal coherence and the resulting spatiotemporal noise features on the stability of spatial soliton arrays generated in a pulsed regime through spatial modulation instability in a nonlinear Kerr planar waveguide. We have considered at the waveguide input a beam composed of a coherent pulse with purely spatial noise deterministic shot to shot, superimposed on a totally spatiotemporally incoherent pulse corresponding to spontaneous parametric downconversion issued from a type 1 BBO quadratic crystal. Because of the presence of random incoherent noise, the soliton arrays therefore present a shot-to-shot spatial jitter in the free transverse dimension of the Kerr waveguide. However, we have numerically demonstrated that the amplitude of this jitter depends both on the spatiotemporal coherence of the input beam and on the relaxation time of the nonlinear Kerr response. The experimental observations confirm the simulations.

The spatial coherence acts directly on the amplitude of the spatial jitter because the degree of correlation between the spatial noise frequency spectra from one shot to another decreases with the spatial coherence. Then, for a fixed degree of spatial coherence, temporal incoherence also perturbs the maintaining of the soliton array along a single pulse.

First, in an instantaneous Kerr medium, the successive temporal slices in one pulse are uncorrelated and they are all the more independent as temporal coherence is low. The consequence for a low temporal coherence is an important blur of the single-shot time-integrated waveguide

output (on a CCD camera, for example) as the transverse spatial position of the bright peaks generated in each temporal slice is strongly fluctuating. On the other hand, the array can remain well contrasted for higher temporal coherence but with a shot-to-shot spatial jitter depending on the spatial coherence. In conclusion, in an instantaneous medium, the jitter amplitude depends only on the spatial coherence while the temporal coherence acts only on the blur of the time-integrated waveguide output profile. This leads us to retrieve and explain the observations made in AlGaAs by Malendevich *et al.* using a partially coherent pulse delivered by an optical parametric generator.[12] In our case, temporal and spatial coherence are correlated as they come essentially from the same noise source (SPDC). Therefore, an increase in temporal coherence to raise the visibility of the soliton arrays corresponds also to an increase in the spatial coherence that would decrease the spatial jitter.

Second, for a noninstantaneous reorientational Kerr medium like CS_2, the temporal slices are correlated by the relaxation time of the Kerr response. Therefore, both the random and the deterministic noise contributions are time integrated on correlation cells whose duration typically equals the relaxation time. This process strongly limits the shot-to-shot spatial jitter. Indeed, for a same noise level, the time integration of the purely spatial deterministic noise (and therefore purely temporally coherent) over the relaxation time gives a greater contribution than the time integration of the spatiotemporal SPDC noise, which is temporally uncorrelated. Then, even if the spatial jitter would be large in an instantaneous medium, this jitter is reduced in a noninstantaneous medium presenting a relaxation time of the same order of magnitude as the pulse duration. Moreover, if the correlation cells are shorter than the pulse duration, the soliton array is not maintained all along the pulse but presents some twisting solitons as the cells are uncorrelated. This temporal twisting effect can completely split the soliton arrays along the pulse if the temporal coherence is too low. A partially blurred time-integrated single-shot waveguide output is thus obtained.

Now, if we superpose coherent and incoherent pulses of different durations, a more complex dynamics occurs. In our case, the incoherent pulse is shorter than the coherent one. Then, to observe the maximal spatial jitter, the incoherent beam has to be synchronized with the front part of the soliton arrays, where MI is more efficient. However, a part of the coherent pulse is not perturbed by the incoherent pulse and then gives a soliton array that is spatially stable shot to shot. Again, this dynamics further decreases the spatial jitter of the soliton arrays. Note that, as already demonstrated in Ref. 15, a perfect stability of the soliton arrays is retrieved both along one pulse and from shot to shot in the absence of an incoherent part, i.e., with only purely spatial deterministic noise.

To uncorrelated the spatial and the temporal noise contributions so as to observe much larger spatial jitter in a relaxing medium, it would be interesting to make experimental measurements with pulses having a duration shorter than the relaxation time of the nonlinear medium. SPDC would then become temporally coherent, which would therefore cancel the twisting soliton effect (a single temporal correlation cell during the pulse). Moreover, in this case, time integration would affect identically the random and deterministic noise. The spatial jitter of the soliton arrays, which depends only on the spatial coherence of the input beam, should therefore be more important at high SPDC levels.

To conclude, this paper contributes to further enlightening the current knowledge on SMI dynamics in practical pulsed situations, both for instantaneous or for relaxing nonlinearities. It shows that, in these situations, usually less-considered parameters like the determinism or the randomness of noise that are linked to the spatiotemporal coherence of the optical field gain strong importance and have a strong effect on the SMI dynamics, the spatiotemporal coupling effects, and the stability of the generated solitonlike structures.

ACKNOWLEDGMENTS

This work has been supported in part by the European Union under the QUANTIM project (contract IST-2000-26019).

The e-mail address for G. Fanjoux is gil.fanjoux@univ-fcomte.fr.

REFERENCES

1. V. I. Bespalov and V. I. Talanov, "Filamentary structure of light beams in nonlinear liquids," JETP Lett. **3**, 307–310 (1966).
2. A. Hasegawa and W. F. Brinkman, "Tunable coherent IR and FIR sources utilizing modulational instability," IEEE J. Quantum Electron. **QE-16**, 694–697 (1980).
3. A. Hasegawa, "Generation of a train of soliton pulses by induced modulational instability in optical fibers," Opt. Lett. **9**, 288–290 (1984).
4. G. P. Agrawal, *Nonlinear Fiber Optics*, 3rd ed. (Academic, 2001).
5. E. M. Dianov, P. V. Mamyshev, A. M. Prokhorov, and S. V. Chernikov, "Generation of a train of fundamental solitons at a high repetition rate in optical fibers," Opt. Lett. **14**, 1008–1010 (1989).
6. H. Maillotte, J. Monneret, A. Barthélémy, and C. Froehly, "Laser beam self-splitting into solitons by optical Kerr nonlinearity," Opt. Commun. **109**, 265–271 (1994).
7. A. V. Mamaev, M. Saffman, D. Z. Anderson, and A. A. Zozulya, "Propagation of light beams in anisotropic nonlinear media: from symmetry breaking to spatial turbulence," Phys. Rev. A **54**, 870–879 (1996).
8. R. A. Fuerst, D.-M. Baboiu, B. Lawrence, W. E. Torruellas, G. I. Stegeman, S. Trillo, and S. Wabnitz, "Spatial modulational instability and multisolitonlike generation in a quadratically nonlinear optical medium," Phys. Rev. Lett. **78**, 2756–2759 (1997).
9. E. Garmire, R. Y. Chiao, and C. H. Townes, "Dynamics and characteristics of the self-trapping of intense light beams," Phys. Rev. Lett. **16**, 347–349 (1966).
10. V. E. Zakharov and A. B. Shabat, "Exact theory of two-dimensional self-focusing and one-dimensional self-modulation of waves in nonlinear media," Sov. Phys. JETP **34**, 62–69 (1972).
11. D. Kip, M. Soljacic, M. Segev, S. M. Sears, and D. N. Christodoulides, "(1+1)-Dimensional modulation instability of spatially incoherent light," J. Opt. Soc. Am. B **19**, 502–512 (2002).
12. R. Malendevich, L. Jankovic, G. Stegeman, and J. S. Aitchison, "Spatial modulation instability in a Kerr slab waveguide," Opt. Lett. **26**, 1879–1881 (2001).
13. W. Krolikowski, O. Bang, J.-J. Rasmussen, and J. Willer,

"Modulational instability in nonlocal Kerr media," Phys. Rev. E **64**, 016612 (2001).
14. C. Cambournac, H. Maillotte, E. Lantz, J. M. Dudley, and M. Chauvet, "Spatiotemporal behavior of periodic arrays of spatial solitons in a planar waveguide with relaxing Kerr nonlinearity," J. Opt. Soc. Am. B **19**, 574–585 (2002).
15. E. Lantz, C. Cambournac, and H. Maillotte, "Spatiotemporal dynamics of soliton arrays generated from spatial noise in a planar waveguide with relaxing Kerr nonlinearity," Opt. Express **10**, 942–948 (2002).
16. H. Leblond and C. Cambournac, "Spatial modulation instability of coherent light in a weakly-relaxing Kerr medium," J. Opt. A Pure Appl. Opt. **6**, 461–468 (2004).
17. M.-F. Shih, C.-C. Jeng, F.-W. Sheu, and C.-Y. Lin, "Spatiotemporal optical modulation instability of incoherent light in noninstantaneous nonlinear media," Phys. Rev. Lett. **88**, 133902 (2002).
18. G. Fanjoux, F. Devaux, E. Lantz, and H. Maillotte, "The generation of spatial soliton arrays in a planar Kerr waveguide from seeded spontaneous parametric down conversion," J. Opt. A Pure Appl. Opt. **6**, S250–S257 (2004).
19. M. Soljacic, M. Segev, T. Coskun, D. N. Christodoulides, and A. Vishwanath, "Modulation instability of incoherent beams in non-instantaneous nonlinear media," Phys. Rev. Lett. **84**, 467–470 (2000).
20. H. Buljan, A. Siber, M. Soljacic, and M. Segev, "Propagation of incoherent 'white' light and modulation instability in non-instantaneous nonlinear media," Phys. Rev. E **66**, 035601(R) (2002).
21. D. Kip, M. Soljacic, M. Segev, E. Eugenieva, and D. N. Christodoulides, "Modulation instability and pattern formation in spatially incoherent light beams," Science **290**, 495–498 (2000).
22. J. Klinger, H. Martin, and Z. Chen, "Experiments on induced modulational instability of an incoherent optical beam," Opt. Lett. **26**, 271–273 (2001).
23. T. Schwartz, T. Carmon, H. Buljan, and M. Segev, "Spontaneous pattern formation with incoherent white light," Phys. Rev. Lett. **93**, 223901 (2004).
24. A. Mussot, E. Lantz, H. Maillotte, and T. Sylvestre, "Spectral broadening of a partially CW laser beam in single-mode optical fibers," Opt. Express **12**, 2838–2843 (2004).
25. A. Sauter, S. Pitois, G. Millot, and A. Picozzi, "Incoherent modulation instability in instantaneous nonlinear Kerr media," Opt. Lett. **30**, 2143–2145 (2005).
26. H. Fang, R. Malendevich, R. Schiek, and G. I. Stegeman, "Spatial modulational instability in one-dimensional lithium niobate slab waveguides," Opt. Lett. **25**, 1786–1788 (2000).
27. L. Jankovic, S. Polyakov, G. Stegeman, S. Carrasco, L. Torner, C. Bosshard, and P. Gunter, "Complex soliton-like pattern generation in Potassium Niobate due to noisy, high intensity, input beams," Opt. Express **11**, 2206–2210 (2003).
28. D. Wang, R. Barille, and G. Rivoire, "Influence of soliton propagation on the beam-polarization dynamics in a planar waveguide," J. Opt. Soc. Am. B **15**, 2731–2737 (1998).
29. H. G. Winful, "Polarization instabilities in birefringent nonlinear media: application to fiber-optic devices," Opt. Lett. **11**, 33–35 (1986).
30. A. Yariv, *Quantum Electronics*, 3rd ed. (Wiley, 1989).
31. N. N. Akhmediev, "Spatial solitons in Kerr and Kerr-like media," Opt. Quantum Electron. **30**, 535–569 (1998).